MATERIALS SCIENCE

Stretchable self-healable semiconducting polymer film for active-matrix strain-sensing array

Jin Young Oh[1,2]*, Donghee Son[1,3,4]*, Toru Katsumata[1,5]*, Yeongjun Lee[6], Yeongin Kim[1], Jeffrey Lopez[1], Hung-Chin Wu[1], Jiheong Kang[1], Joonsuk Park[7], Xiaodan Gu[1,8], Jaewan Mun[1], Nathan Ging-Ji Wang[1], Yikai Yin[7], Wei Cai[9], Youngjun Yun[1,10]†, Jeffrey B.-H. Tok[1], Zhenan Bao[1]†

Skin-like sensory devices should be stretchable and self-healable to meet the demands for future electronic skin applications. Despite recent notable advances in skin-inspired electronic materials, it remains challenging to confer these desired functionalities to an active semiconductor. Here, we report a strain-sensitive, stretchable, and autonomously self-healable semiconducting film achieved through blending of a polymer semiconductor and a self-healable elastomer, both of which are dynamically cross-linked by metal coordination. We observed that by controlling the percolation threshold of the polymer semiconductor, the blend film became strain sensitive, with a gauge factor of 5.75×10^5 at 100% strain in a stretchable transistor. The blend film is also highly stretchable (fracture strain, >1300%) and autonomously self-healable at room temperature. We proceed to demonstrate a fully integrated 5 × 5 stretchable active-matrix transistor sensor array capable of detecting strain distribution through surface deformation.

INTRODUCTION

Recent progress in stretchable electronic materials (*1*, *2*) and devices (*3*, *4*) that emulate the sensing and self-healing properties of human skin has accelerated the development of skin-inspired devices, soft robots, and biomedical devices (*5*–*14*). Various rigid sensing modules have been integrated into an ultrathin platform using strain-engineered designs for interconnects and fabrication by transfer printing (*15*, *16*). Bioinspired structures/materials are created to further improve sensitivity and compatibility with the human body (*2*, *17*, *18*). A modulation of mechanical stimuli to electrical signals has been a representative function of the electronic skin (e-skin), which mimics the human skin sensory function (*3*, *19*).

The active-matrix transistor array–based sensors provide high-quality sensing signals with reduced cross-talk between the individual pixels (*20*–*26*). In this case, each pixel consists of a sensor connected with a transistor. Previous works used strain engineering to integrate rigid sensors and transistors into stretchable biomimetic systems (*4*, *7*). To overcome mechanical mismatch between rigid and soft components, both sensors and transistors need to be intrinsically stretchable. Stretchable semiconductor that shows strain-dependent electrical behavior is a potential candidate that combines sensing and transistor switching. Such a strain-sensing transistor can potentially simplify fabrication processes and improve mechanical robustness and conformability. In addition, a self-healing ability would be an added benefit to e-skin to warrant a longer lifetime of the e-skin (*27*–*38*).

Here, we present an intrinsically stretchable and self-healable semiconducting film that has strain-sensitive electrical behavior when incorporated into a stretchable transistor. The semiconducting film was prepared by a blend of polymer semiconductor and an insulating elastomer. Both materials, which contain metal ligand dynamic bonding sites, were recently reported by our group for stretchable and self-healable electronic materials (*6*, *30*). Here, we intend to demonstrate a new property by fusing the two materials together for strain-sensitive semiconducting film through dynamic cross-linking of polymer semiconductor and insulating elastomer. The metal coordination bond, once broken, can spontaneously reconstruct, rendering the brittle semiconducting film stretchable, tough, and self-healing. Moreover, the elastomer in the blended film is highly elastic with low modulus, effectively absorbing the external mechanical strain conferred. Thus, this approach can be a new way for developing multifunctional electronic materials.

The strain sensitivity that is defined as its field-effect mobility modulation of the semiconducting film to external stimuli can be optimized by controlling the weight ratio of the semiconducting polymer and insulating elastomer. The nanoparticle-like phase separation of the semiconducting film enabled it to be further strain sensitive, since the local distance between zero-dimensional (0D) structures is highly correlated to the effective charge transportation during stretching and releasing (*39*–*42*). The optimized semiconducting film showed high strain sensitivity [gauge factor (GF), 5.75×10^5 at 100% strain] and intrinsic stretchability (fracture strain, >1300% strain; fig. S2). The GF was calculated as a general equation for piezoresistive semiconductor and conductor, $GF = (\Delta R/R)/\varepsilon$, and the method is further explained in the Materials and Methods section. In addition, the broken dynamic bonding can be spontaneously reformed, enabling the recovery of the damaged film. The cut semiconducting film was observed to be autonomously self-healed after 1 day at room temperature, and its field-effect mobility was almost completely recovered. Next, we fabricated a crack-based stretchable gold (Au) nanomembrane interconnector that is highly conductive and durable up to 100% strain according to literature report (*43*). Last, we proceeded to fabricate a stretchable active-matrix sensory transistor

[1]Department of Chemical Engineering, Stanford University, Stanford, CA 94305-5025, USA. [2]Department of Chemical Engineering, Kyung Hee University, Yongin 17104, South Korea. [3]Biomedical Research Institute, Korea Institute of Science and Technology, 5, Hwarang-ro 14-gil, Seongbuk-gu, 02791 Seoul, South Korea. [4]School of Electronic and Electrical Engineering, Sungkyunkwan University, Suwon 16419, South Korea. [5]Corporate Research and Development, Performance Materials Technology Center, Asahi Kasei Corporation, 2-1 Samejima, Fuji, Shizuoka 416-8501, Japan. [6]Department of Materials Science and Engineering, Seoul National University, Seoul 08826, Republic of Korea. [7]Department of Materials Science and Engineering, Stanford University, Stanford, CA 94305-5025, USA. [8]School of Polymer Science and Engineering, The University of Southern Mississippi, Hattiesburg, MS 39406, USA. [9]Department of Mechanical Engineering, Stanford University, Stanford, CA 94305-5025, USA. [10]Samsung Advanced Institute of Technology Yeongtong-gu, Suwon-si, Gyeonggi-do 443-803, South Korea.
*These authors contributed equally to this work
†Corresponding author. Email: zbao@stanford.edu (Z.B.); youngjun.yun@samsung.com (Y.Y.)

array. The semiconducting film, dielectric, electrode, and interconnect are all effectively integrated into an active-matrix array platform using a transfer-printing process. Our stretchable active-matrix skin-like sensor array is successfully capable of monitoring strain distribution of the external force. In addition, a transfer-printed passivation layer enabled the semiconductor/dielectric interface of the sensor array to be waterproof even after we drop-casted artificial sweat on it for 15 hours. Our demonstrated strain-sensitive, stretchable, and self-healable semiconducting film would change the paradigm of the e-skin to further expand its application.

RESULTS AND DISCUSSION

Figure 1 shows the overall material design strategy for the strain-sensitive, stretchable, and self-healable semiconducting film and its mechanical and electrical properties. We choose poly(3,6-di(thiophen-2-yl)diketopyrrolo[3,4-c]pyrrole- 1,4-dione-alt-1,2-dithienylethene) with 10 mol% 2,6-pyridinedicarboxamine moieties (DPP-TVT-PDCA) as the semiconducting material due to its good charge carrier mobility, as we reported previously (*6*), and the PDCA units that can be used to bind to the insulating and stretchable poly(dimethylsiloxane-alt-2,6-pyridinedicarbozamine) (PDMS-PDCA) polymer (Fig. 1A) (*30*).

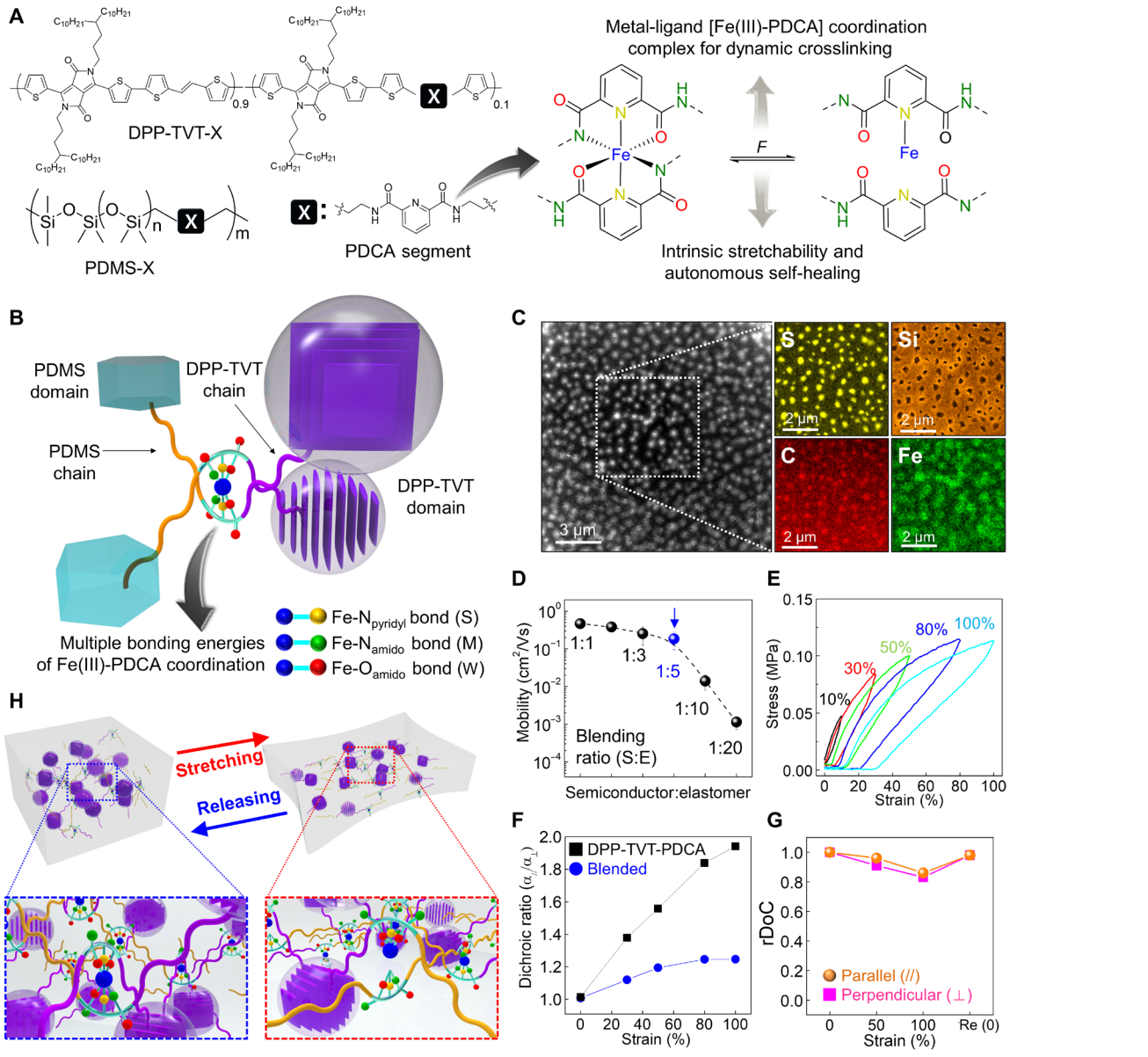

Fig. 1. Design and characterizations of strain-sensitive, stretchable, and self-healable semiconducting film. (**A**) Chemical structure of DPP semiconducting polymer, PDMS, and PDCA moiety introduced in both polymer backbones as dynamic bonding sites through metal-ligand interaction. Structure of the $[Fe(HPDCA)_2]^+$ moiety that is reversible dynamic bonds by force. (**B**) Schematic illustration of DPP and PDMS dynamically cross-linked through Fe(III)-PDCA complexation. (**C**) STEM dark-field and STEM-EDS elemental mapping of the DPP-TVT-PDCA (1):PDMS-PDCA-Fe (5) blend film. (**D**) Field-effect mobilities of the blend film organic thin-film transistors (OTFTs) (source and drain electrode: Au, 40 mn; dielectric layer: SiO_2, 300 nm; gate electrode: highly doped silicon substrate) as a function of blending-weight ratio (semiconductor:elastomer). (**E**) Strain cyclic testing of the blend film (1:5). (**F**) Plot of dichroic ratio ($\alpha_{//}/\alpha_{\perp}$) of 1:5 blend film as a function of strain. (**G**) Relative degree of crystallinity (rDoC) calculated from (200) peak for both "parallel" and "perpendicular" directions to x-ray beam line. (**H**) Proposed mechanism for reinforcement of stretchability in blend film via metal-ligand dynamic bonding based on analyzed information.

We previously reported the use of PDCA to form metal-ligand coordination complex with a molar ratio of Fe(III) ion to PDCA ligand of 1:2 (*30*). It was shown that Fe(III)-PDCA coordination has multiple dynamic bonds with three different bonding strengths (Fe-$N_{pyridyl}$, strong; Fe-N_{amido}, medium; and Fe-O_{amido}, weak) facilitating the dynamic cross-linking for intrinsic stretchability and self-healing ability (*30*). The metal-ligand coordination bond was formed first during the preparation of PDMS-PDCA-Fe elastomer [PDCA:Fe(III) = 2:1] to prevent chemical damage of the semiconducting polymer from a strong acidic by-product (hydrochloric acid). The semiconducting film was prepared by blending semiconducting DPP-TVT-PDCA and PDMS-PDCA-Fe elastomer. The cross-linked PDMS-PDCA-Fe chains in organic solvent can exchange metal-ligand bonding with PDCA segment in DPP-TVT chains. Figure 1B shows a schematic illustration of Fe(III)-PDCA ligand bonding of PDMS-PDCA and DPP-TVT-PDCA in the blend film.

We evaluated the dependency of field-effect mobility on semiconductor (DPP-TVT-PDCA), with an elastomer (PDMS-PDCA-Fe) weight ratio ranging from 1:1 to 1:20, as shown in Fig. 1D and fig. S1. The optimized weight ratio of the blend film was observed to be 1:5, which is the minimum weight ratio of the semiconducting polymer to give reasonable charge carrier mobilities, which suggest that sufficient electrical percolation paths (highlighted in blue color in Fig. 1D) are still preserved in the blend film. The observed volume faction was 0.166, as determined by sulfur element, indicating semiconducting polymer in Fig. 1C using ImageJ software. This value is very close to the theoretical percolation threshold volume fraction of 0.16 for spherical particles (*44*). The blend film was observed to have a high stretchability (fracture strain, >1300%; fig. S2) with a Poisson's ratio of 0.462 (fig. S3), and its Young's modulus (~300 kPa) is similar to that of human skin, while typical semiconducting polymers are in the range of hundreds of megapascals to gigapascals (*45*). Next, the rheology analysis of the blend film at room temperature showed that the storage modulus (G') is higher than the loss modulus (G'') in a typical frequency range from 10^{-3} to 10^{3} Hz and a temperature range from 10° to 60°C, respectively, which indicates that the blend film behaves like a solid material due to the metal-ion coordination cross-linking with the more rigid DPP-TVT (figs. S4 and S5). In addition, the low glass transition temperature of the blend film (below −90°C; fig. S6) is similar to that of typical PDMS rubber (*46*). To further analyze the stretchability of the blend film, we conducted a repeated strain cyclic test, as shown in Fig. 1E. We observed that the blend film began to display stress-strain hysteresis when it was stretched to above 30% strain. We attribute this hysteresis to energy dissipation, resulting from the breakage of Fe(III)-PDCA coordination bonds, leading to stress relaxation (fig. S7). However, even when the blend film was elongated by stretching it to over 100% strain, we observed that it was able to revert to its initial length after 1 hour of rest (fig. S8). This recovery is attributed to the reorganization of the polymer chains to, approximately, their initial configurations driven by the energetic gain of the configurational entropy of this initial state.

To characterize the electrical percolation path in the blend film, the morphology of the blend film was characterized by transmission electron microscopy (TEM). The morphology of the blend film depended on the blend ratio from 1:1 to 1:20 (semiconductor:elastomer; fig. S9). We observed nanoparticles uniformly distributed in the 1:5 blend film on the order of 100 nm. These nanoparticles were formed during thermal annealing through phase separation driven by difference of surface energy of the two different materials. Element mapping of the scanning TEM (STEM) image was subsequently performed by energy-dispersive x-ray spectroscopy (EDS) to identify elements in the film (Fig. 1C). Sulfur (S) and silicon (Si) peaks are used to determine the presence of semiconducting and insulating polymers, respectively (see chemical structures in Fig. 1A). In the nanoparticle regions, strong S and Fe signals can be seen, while other regions showed strong Si signals. These results indicate that the nanoparticles are primarily composed of the semiconducting polymers with Fe-PDCA, potentially at the interface between the semiconducting domains and the PDMS regions. Although the connection between the nanoparticle semiconducting domains cannot be seen clearly, the charge carrier mobility still maintained a value as high as 0.1 cm^2/Vs. This suggests that the nanoparticles are connected by a small amount of DPP-TVT. This also suggests that the blend film maybe very sensitive to strain.

To characterize the molecular level changes of the semiconducting polymer during stretching, the chain alignment was measured using polarized ultraviolet-visible (UV-vis) spectroscopy (fig. S10), and the degree of chain alignment was quantified in terms of its dichroic ratio ($\alpha_{//}/\alpha_{\perp}$), as shown in Fig. 1F. The dichroic ratio of the blend film was observed to linearly increase up to 50% strain (presumably due to strain-induced chain alignment) and plateaued at 100% strain, while the neat semiconducting polymer's dichroic ratio linearly increased up to 100% with a higher slope. The observed difference in response to strain is may be because the elastomer is easier to stretch by strain due to its lower modulus than the semiconducting polymer in the blend film.

The relative degree of crystallinity of the blend film was measured using grazing-incidence wide-angle x-ray diffraction to understand the change of film morphology upon stretching cycles (Fig. 1G and figs. S11 and S12). The initial crystallinity of blend film was maintained at ~80%, although it was stretched up to 100% strain and fully recovered regardless of stretching direction with preserving full-width at half maximum value (parallel and perpendicular stretching directions to x-ray beam). This observation, together with the dichroic results, indicates that the applied strain is mainly absorbed into the elastomer while preserving the crystalline regions of the semiconducting polymer. Together, this constitutes the proposed stretching mechanism of the blend film (Fig. 1H).

To evaluate the strain-sensitive charge transport of the semiconducting film, organic thin-film transistors (OTFTs) were fabricated using transfer printing of the semiconducting film (200 nm), as shown in Fig. 2A. The semiconducting film was stretched from 0 to 100% strain on PDMS elastomer stamp and transferred onto the surface of SiO_2 (dielectric) on a heavily doped Si (gate) substrate. Atomic force microscopy (AFM) images did not find any nanocracks in the transferred film, indicating no mechanical damage due to strain (Fig. 2B). Gold, as an electrode material, was then thermally evaporated on the blend film. The OTFT showed typical transistor output and transfer curves (fig. S13). They were observed to be highly sensitive on-current as a function of the applied strain. Specifically, the on-current of the transistor decreased from 2.79×10^{-5} A at 0% strain to 4.85×10^{-10} A at 100% strain (Fig. 2C). The GF was 5.75×10^{5} at 100% strain (Fig. 2D), which is among the highest values previously reported for semiconducting strain gauges and even comparable with the state-of-art conductor-based strain gauges. As a comparison, the highest value previously reported were for graphene-polymer nanocomposite-based strain sensors and mechanical crack-based strain sensors, which showed GFs of more than 500 and 2000 (0 to 2% strain), respectively

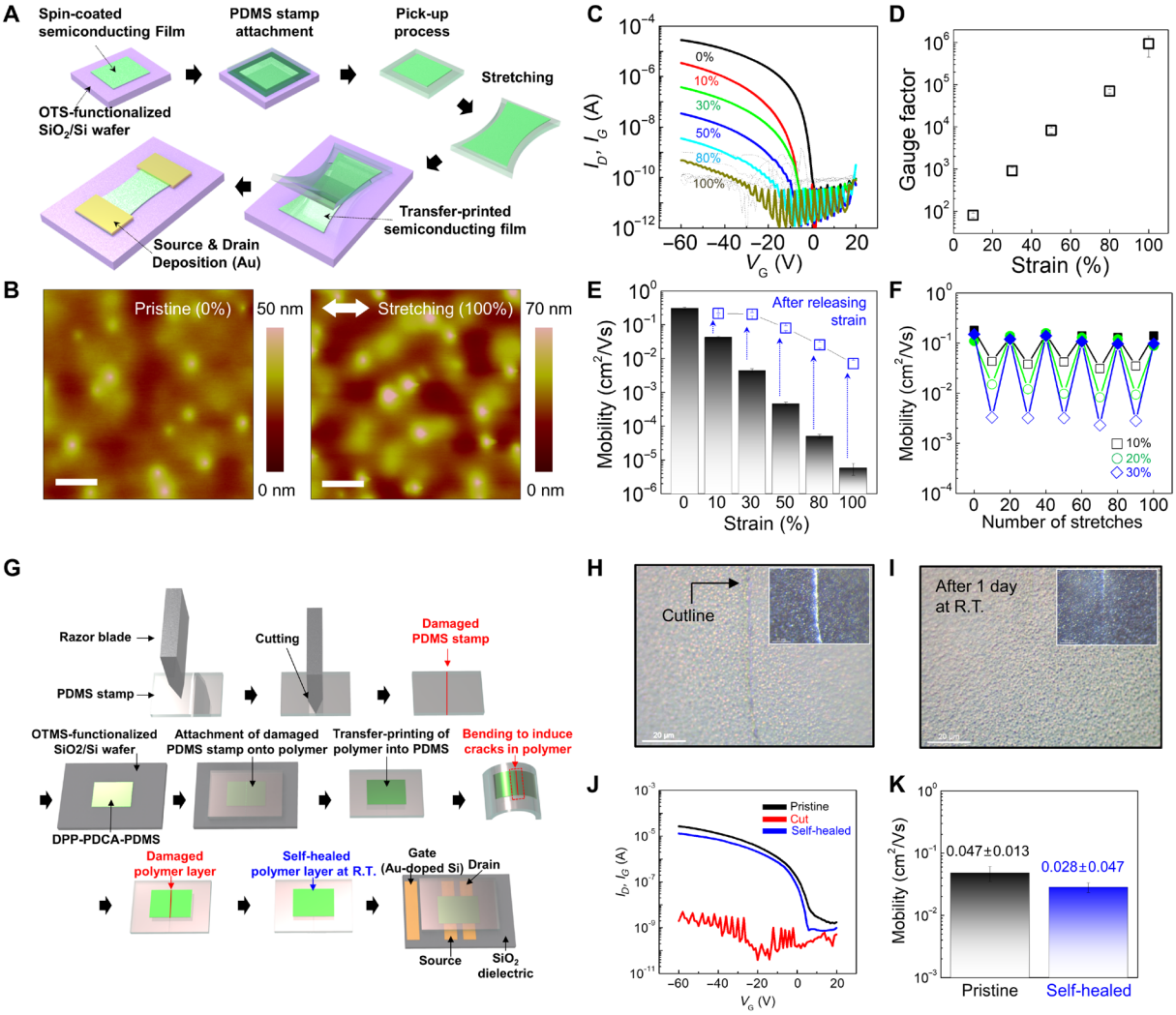

Fig. 2. Strain-sensitive property of self-healable semiconducting film. (**A**) Schematic illustration for sequential fabrication procedures of the OTFT with stretchable self-healable semiconducting film (200 nm) using transfer-printing assembly. (**B**) AFM height images for pristine and stretched (100%) semiconducting films. Scale bars, 1 μm. (**C**) Transfer curves of OTFTs as a function of strain applied to semiconducting film along the tensile stretching direction and (**D**) GFs extracted from on-current of OTFTs. (**E**) Field-effect mobilities on strain and after releasing strain measured for the same device. (**F**) Field-effect motility as a function of stretching cycle at different strains. (**G**) Schematics for fabrication methods of the self-healed semiconducting film that was cut by bending a partially cracked PDMS stamp and its OTFT. (**H**) Optical microscope (OM) images of damaged semiconducting film through self-healing process and (**I**) self-healed film. Inset: Corresponding dark-field OM images. (**J**) Transfer curves and (**K**) field-effect mobility of pristine and autonomously healed OTFTs. R.T., room temperature.

(*47*–*50*). The morphology of the blend film, as observed by optical microscopic images and AFM, during stretching did not show any visible cracks up to 100% strain (fig. S14). The devices showed fully reversible current-voltage characteristics (Fig. 2E) and repeatable cycling behavior within a strain range of 30% (Fig. 2F and fig S15), a value similar to the stretchability of human skin.

Self-healing is a unique function for next-generation e-skin. Our semiconducting film can be self-healed through the dynamic metal-ligand coordination bonding. To evaluate the film's self-healing ability, the blend film (200 nm in thickness) was cut and left at room temperature. After 24 hours, we observed the scar of the cut film autonomously disappeared, i.e., self-healed. Furthermore, the healed film could be stretched again to more than 200% strain before fracturing (fig. S16). Since the thickness of the semiconducting layer in a thin film transistor is only on the order of tens of nanometers, it needed to be supported by a substrate for cutting and self-healing tests. Figure 2G shows a process to perform these tests. Briefly, the self-healable semiconducting film was transferred to a precut PDMS stamp from an octadecyl trichlorosilane (OTS)–treated SiO_2/Si substrate and then was broken by bending the semiconducting film/PDMS stamp quickly. The two broken pieces of semiconducting films were thus self-aligned to contact with each other when the PDMS substrate was returned to a flat structure (Fig. 2G). Figure 2H depicts an optical microscope image of the semiconducting film (200 nm) after breaking on the stamp. For autonomous self-healing, the damaged film was left without any post-treatment at room temperature. The scar in the damaged film was observed to be completely gone after self-healed for 1 day (Fig. 2I). Next, the electrical property of the healed semiconducting film was evaluated in a bottom-contact bottom-gate–structured OTFT shown in Fig. 2G using a soft-contact

method. Figure 2J shows the transfer curves before and after self-healing, in which the field-effect mobility of the healed semiconducting film was recovered from 0.047 ± 0.013 to 0.028 ± 0.047 cm^2/Vs (Fig. 2K). In comparison, the device with cut semiconducting film without allowing to self-heal did not show any transistor-like current-voltage behavior.

To demonstrate the potential of our newly developed semiconducting film for e-skin applications, we proceeded to fabricate a 5 by 5 fully stretchable strain-sensitive active-matrix transistor array (Fig. 3). Typically, resistive sensors require an active-matrix backplane for multiplexing without cross-talk between pixels. The use of the above strain-sensitive transistors combines a strain-resistive sensor and a transistor into one single device and reduces the complexity in device fabrication and potentially gives higher sensitivity. To achieve high-speed scanning of multiple lines without signal delay or loss in the active-matrix architecture, a highly stretchable and conducting interconnect is required. Although many stretchable electrodes have been reported using nanowires or nanotubes, or nano/microparticles, these approaches generally involve a trade-off between electrical conductivity and mechanical stretchability. Recently, a wrinkled and cracked metal nanomembrane supported on elastomer substrates was reported for stretchable electrodes (*4*,*43*,*51*,*52*). Building on this concept, we further developed highly conductive stretchable electrode using Au and polystyrene-block-poly(ethylene-ran-butylene)-block-polystyrene (SEBS) elastomer for the interconnect of active-matrix transistor array. Figure 3A shows a plot of resistance of the Au (thickness of 80 nm) nanomembrane/SEBS free-standing electrode as a function of time with different tensile strains (black, 50%;

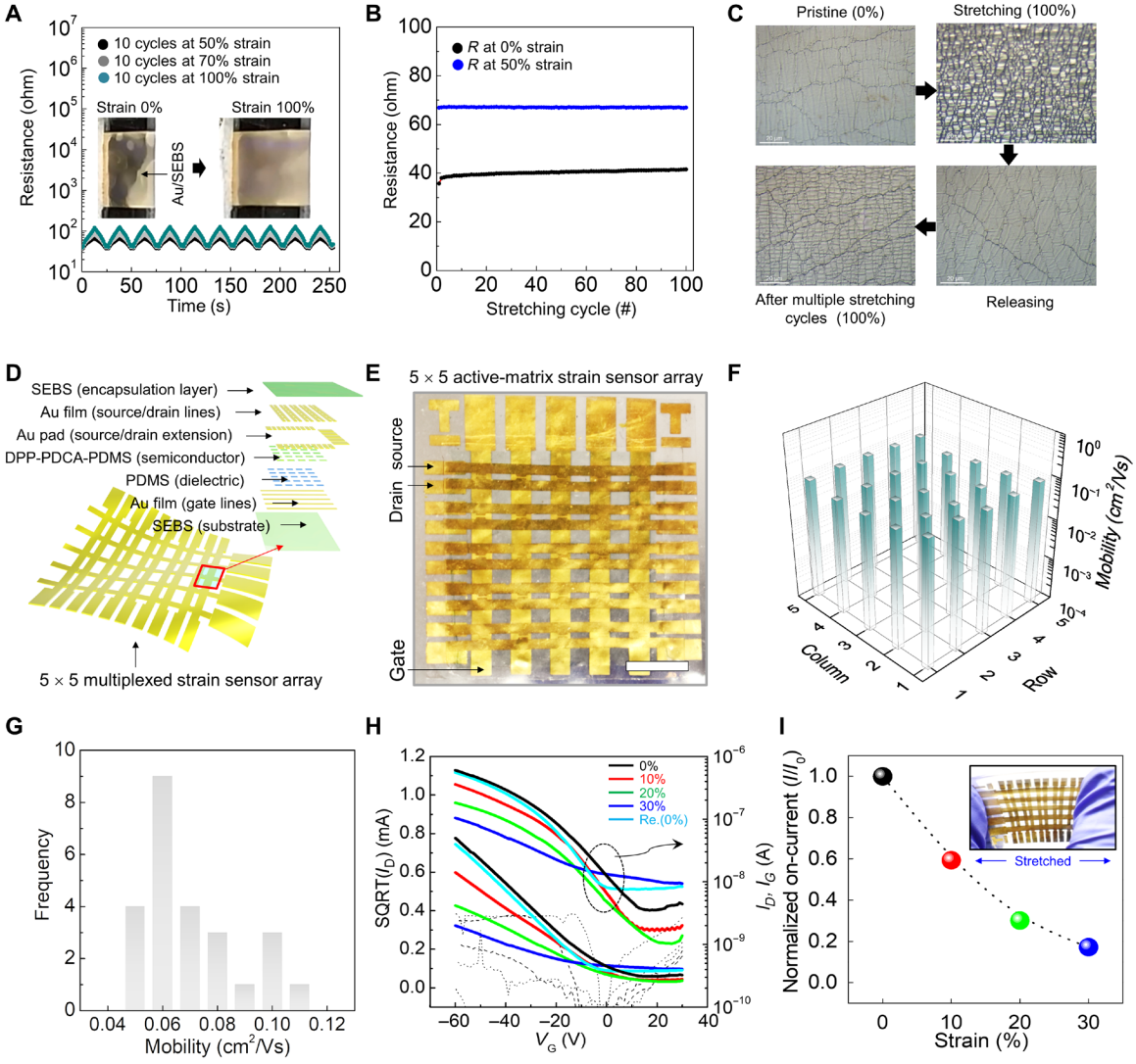

Fig. 3. Characterizations of stretchable active-matrix transistor sensor array. (**A**) In situ measurement of resistance of Au/SEBS stretchable interconnect during 10 stretching cycles at different strains (50, 70, and 100%). Inset: Photographs of Au/SEBS interconnect at 0% (left) and 100% (right) strain. (**B**) Resistance change of Au/SEBS stretchable interconnect as a function of stretching cycle at 0 and 50% strain. (**C**) OM images of pristine (0% strain, upper left), stretched (100% strain, upper right), released (0% strain, lower right), and stretched (100% strain; 100 cycles, lower left) Au/SEBS stretchable interconnect. (**D**) Architecture and (**E**) photograph of a fully stretchable 5 × 5 active-matrix transistor strain sensor array fabricated via our developed strain-sensitive, stretchable, and self-healable semiconducting film. Scale bar, 5 mm. (**F**) Mapping and (**G**) statistical distribution of the field-effect mobility in our stretchable active-matrix transistor array. (**H**) Transfer curves and (**I**) normalized on-current of fully stretchable transistor in active-matrix array as a function of strain. Photo credits: Jin Young Oh, Department of Chemical Engineering, Kyung Hee University and Donghee Son, Biomedical Research Institute, Korea Institute of Science and Technology. SQRT, square root.

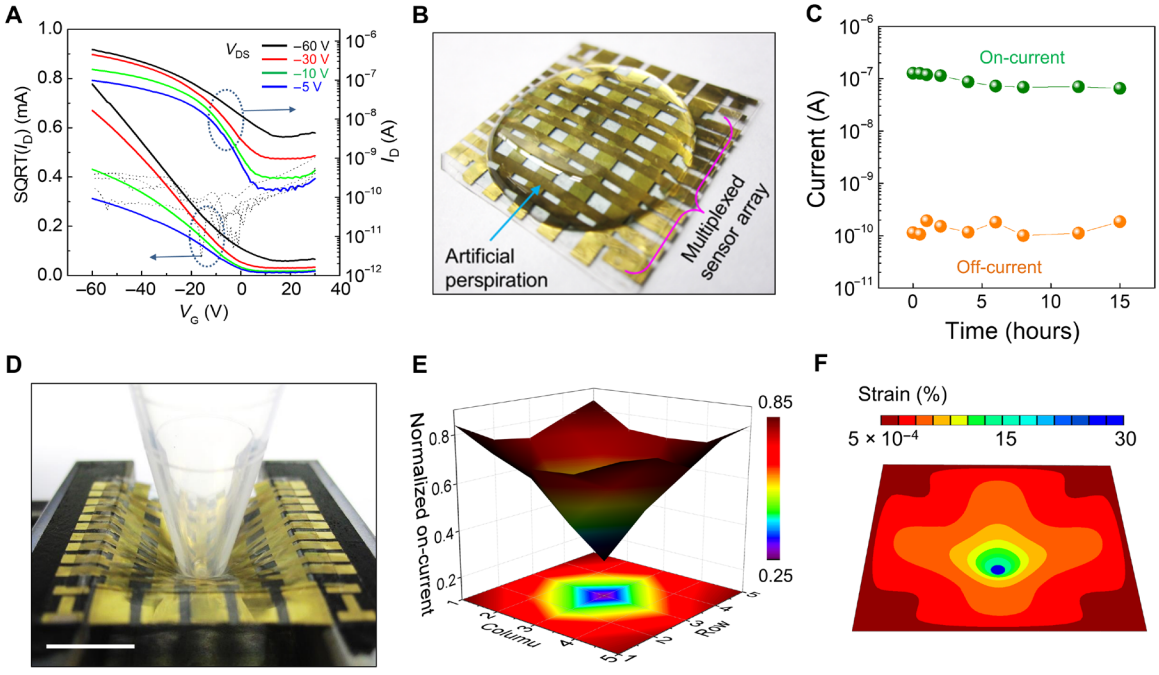

Fig. 4. Strain-sensitive stretchable active-matrix transistor array as skin-like stretchable strain sensor. (**A**) Transfer curves of the stretchable active-matrix transistor array as a function of drain voltage with four different drain/source voltages. (**B**) Photograph of the stretchable active-matrix transistor array under artificial sweat and (**C**) on- and off-currents of the stretchable active-matrix transistor array as a function of time. (**D**) Photograph of stretched active-matrix transistor array by poking with a plastic bar and (**E**) normalized on-current of the poked active-matrix transitory array. (**F**) Simulation result of strain applied by poking to the stretchable active-matrix array. Photo credits: Jin Young Oh, Department of Chemical Engineering, Kyung Hee University.

gray, 70%; teal, 100%) while stretching the electrode for a total of 10 cycles. Inset indicates photographs of the electrode before and after stretching up to 100% strain. Compared to previous electrodes, absolute resistance values are relatively low and stable even at the tensile strain of 100%. To confirm the mechanical reliability of our electrode, we performed repeated cyclic testing up to 100 cycles under 50% strain (Fig. 3B). Superior performance was obtained from the reversible wrinkled and cracked nanostructures supported on a SEBS (elastic modulus, 3.5 MPa) with high elasticity Fig. 3C). The good mechanical and electrical stability of the stretchable interconnect is important to allow good contact to our semiconducting layer via a conventional evaporation process and transfer-printing to give a 5 × 5 strain-sensitive transistor array (Fig. 3, D and E). The active area of each pixel has a channel width of 1 mm and channel length of 150 μm. We observed that all devices showed good uniformity with a maximum mobility of 0.11 cm^2/V s and an average mobility of 0.076 ± 0.019 cm^2/V s (Fig. 3, F and G, and fig. S17). To verify its reversible strain-sensing operations, we stretched the device up to 30% strain and then released it while applying a gate voltage of −60 V at a read voltage of −60 V (Fig. 3H). As expected, the fully stretchable transistor is sensitive to the applied strain, while the saturation drain current was linearly reduced when applied strain was increased. It was also able to fully recover to the original level after the strain was released. Normalized on-current of the device depending on strain is presented in Fig. 3I.

For practical application of the stretchable strain sensor array as e-skin, a lower device-operating voltage is desirable for long-term sustainability and safety. Hence, the drain voltage of device was reduced from −60 to −5 V. Despite the thick dielectric layer, due to the low-threshold voltage, the device still showed ideal transfer curves in accordance to applied drain voltages and was sensitive on applied strain under the reduced drain voltage (−5 V) (Fig. 4A and fig. S18). Next, waterproof performance is highly desirable since the ions from sweat as generated from human skin may result in malfunction of the device. Thus, our fabricated 5 × 5 sensory transistor array was passivated using SEBS elastomer to protect it against sweat (Fig. 4B). The resulting encapsulated device was observed to maintain its electrical performance from undesired leakage sources for a 15-hour operating duration when submersed in artificial sweat (Fig. 4C). The distinctive property of our fabricated active-matrix skin-like sensor array is that this monolithic sensing system enables 3D mapping of e-skin surface deformation with a simplified fabrication process as it combines one sensor and one transistor architecture into one transistor device. To demonstrate its functionality as the stretchable strain sensor, we used a plastic tip to poke on the sensor array (Fig. 4D) while simultaneously recording the on-currents from multiple pixels of the array (Fig. 4E and table S1). The obtained 3D hemispheric shape of the normalized on-current mapping corresponded to that of the "poked" e-skin. To quantify the on-current changes of the active-matrix sensor array upon poking it, we simulated the applied strain using finite-element method. Figure 4F shows a mapping of calculated maximum principal strain on our active-matrix sensor array, which is able to subsequently calibrate the current changes in our device through the calculated principal strains, as shown in fig S19.

CONCLUSION

We present here an approach to enable strain-sensitive, stretchable, and self-healable semiconductor film for fabrication of skin-like active-matrix strain sensor array. We observed that supramolecular

dynamic cross-linked network of semiconducting polymer and a self-healing elastomer provides strain sensitivity to our blended film. In addition, the dynamical cross-linked network by metal-ligand coordination enabled the semiconductor to be not only highly stretchable (>1500%) but also autonomously self-healable at room temperature. The measured GF, an indicator for strain sensitivity of the film, was 5.75×10^5 with up to 100% strain, which is the highest reported value for strain-sensitive semiconducting materials. With these properties, a stretchable active-matrix strain sensor transistor array was designed and fabricated with our semiconducting film. Highly stretchable interconnects were developed to enable reliable data acquisition from the active-matrix sensor. The stretchable active-matrix sensor–based e-skin is able to detect pressure-induced deformation of the e-skin, with simultaneous visualization of the applied strain. Last, for skin-like sensory devices, which are fully self-healable and can be operated within range of medically safe voltage, the integration with self-healable conductor and especially high-*k* dielectric material still need to be developed.

MATERIALS AND METHODS

Material preparations

DPP-TVT-PDCA (10 mol% PDCA segment) and PDMS-PDCA were synthesized according to previously reported methods (*6*, *30*). PDMS diol (Shin-Estu Co.) of number-averaged molecular weight of 100 kDa was used, and the resulting PDMS-PDCA has a number-averaged molecular weight of 11 kDa and a polydispersity of 8.4 determined by gel permeation chromatography (GPC) using polystyrene standards and 1,2,4-trichlorobenzene as eluent at 135°C. PDMS-PDCA-Fe elastomer was prepared using the molar ratio of PDMS-PDCA (Fe of 1:2). Semiconducting DPP-TVT-PDCA has 10 mol% PDCA, a number-averaged molecular weight of 29 kDa, and a polydispersity of 3.0 measured by nuclear magnetic resonance in trichloroethylene at 120°C and GPC using polystyrene as standards and 1,2,4-trichlorobenzene as eluent at 135°C. DPP-TVT-PDCA and PDMS-PDCA-Fe elastomer were dissolved in chlorobenzene (18 mg/ml) with the weight ratio of 1 (DPP-TVT-PDCA) to 5 (PDMS-PDCA-Fe). The blended solution was filtered by syringe filter (1-μm pore size) to remove microscale particles after dissolving on hotplate (90°C) for 1 hour.

Device fabrications

Conventional organic field-effect transistors were fabricated on OTS-treated SiO_2 (dielectric, 300 nm)/Si (gate) substrate. Semiconducting film was coated on the OTS-treated SiO_2/Si using the blend solution. The OTS treatment was carried out according to previous report (*53*). The semiconducting film was then annealed at 170°C for 10 min in vacuum oven. Source and drain electrodes (Au) (thickness, 40 nm; width, 1000 μm; and length, 150 μm) were thermally evaporated in a vacuum chamber at a pressure below 5×10^{-6} torr. Fabrication of stretchable active-matrix transistor sensor array was produced with all stretchable electronic components. SEBS elastomer (SEBS Tuftec H1062 from Ashahi Kasei Co.) was used as stretchable substrate (0.1 mm in thickness) and passivation film (0.1 mm in thickness). Gate electrodes (Au) (thickness, 50 nm; width, 2 mm; and length, 2 cm) were thermally evaporated on SEBS substrate with patterned shadow mask. A PDMS dielectric layer (2.0 μm thick; prepared from 1:2 Sylgard 184 PDMS:crossliker ratio and cured at 75°C for 4 hours) was transferred from an OTS-SiO_2/Si substrate to Au (gate)/SEBS substrate, followed by transferring patterned semiconducting films (thickness, 200 nm; width, 3 mm; length, 3 mm), as shown in fig. S20. Patterned source and drain electrodes (Au) (thickness, 50 nm; width, 1000 μm; and length, 150 μm) were thermally evaporated on a SEBS passivation layer. Last, the SEBS passivation with the source and drain electrode was laminated onto the semiconducting film/PDMS/Au/SEBS substrate, as shown in Fig. 3D.

Characterization

The films were analyzed using optical microscope (LEICA DM4 M), AFM (Digital Instruments), and TEM (FEI Tecnai G2 F20). Rheology experiments were performed using an 8-mm parallel plate as the top geometry and an Advanced Peltier System at 25°C as the bottom geometry (TA Instruments ARES-G2). Stress-strain testing of the materials was carried out using an Intron 5565 load frame, with a 100-N load cell. Stress-relaxation experiments were performed on a DMA Q800 (TA Instruments). Thermal property of materials was measured using differential scanning calorimetry (TA Instruments Q2000). Analysis of crystalline structure of semiconducting film was carried out using grazing-incidence x-ray diffraction. The grazing-incidence x-ray diffraction was conducted at beamlines 11 to 3 of the Stanford Synchrotron Radiation Lightsource. The x-ray wavelength was 0.9758 A corresponding to a beam energy of 12.7 keV. All grazing-incidence x-ray diffraction images were collected in reflection mode with a 2D area detector and the sample under a helium atmosphere. The sample-detector distance was around 300 mm, and the incidence angle was 0.12°. Data analysis was also performed in Wixdiff, written by S. Mannsfeld. The relative degree of crystallinity was performed by normalizing the scattering intensity to scattering volume and exposure time. The scattering intensity was also corrected for scattering geometry, as detailed in previous work by Toney and co-workers (*54*). Dichroic ratios of all films were measured using polarized UV-vis spectroscopy (Cary 6000i Spectrophotometer). Electrical property of devices was measured using the Keithley 4200 parameter analyzer. On-currents of the poked transistor array were measured by manual mode of the Keithley 4200 parameter analyzer, while the plastic bar was poked (poking depth, 5 mm) to the stretchable active matrix with plastic bar at −60 V_{DS} and −60 V_G and the on-currents of the poked transistor array were then normalized by that of the transistor array before poking (0% strain; table S1). Elemental mapping was performed by STEM-EDS to show the elemental distribution of the 1:5 TVT-PDCA:PDMS-PDCA-Fe. STEM-EDS mapping (6 μm by 6 μm) was operated at 200-kV accelerating voltage, with 60-nm spot size. The GF of the strain-sensitive semiconducting layer was calculated with a general equation for piezo-resistive semiconductor and conductor, $GF = (\Delta R/R)/\varepsilon$, where R and ε are resistance and applied strain of piezo-resistive material, respectively. The resistance was converted from on-current of transistor at −60 V_G, whose geometry is top-contact bottom-gate structure (source and drain, Au; dielectric layer, SiO_2; and gate, heavily doped p^{++} silicon substrate). The rigid dielectric and nonstretchable drain and source electrodes were used to minimize potential artifacts from poor electrode contacts and interface delamination during strain to characterize the intrinsic properties of the strain-sensitive semiconducting layer.

Simulation

Using Abaqus 2017, we created a 3D finite-element thin-film structure with the same dimension (27 mm by 27 mm by 0.25 mm) as the stretchable transistor array. To be consistent with experiments, each

of the four edges was clamped over a width of 3.5 mm, leaving an effective deformable area of 20 mm by 20 mm. The mechanical properties of the thin film were dominated by the SEBS substrate because it occupies most of the device volume. As a result, the constitutive relation of the SEBS obtained by fitting the experimental measurement of the stress-strain responses to the Abaqus build-in Ogden model was used as the input material to the finite-element model of the stretchable transistor array (*55*, *56*). The forces acting on the top surface of the film by the poking rod was simulated by traction forces in the contact area. The strain mapping of the deformed thin film was captured after conducting a static analysis until a poking depth of 5 mm is reached. Note that the maximum principle nominal strain was used as a measure of the tensile strain of the stretchable transistor array under poking. The strain distribution predicted by the simulation is in agreement with the strain (normalized on-current) distribution measured by our stretchable strain sensor.

SUPPLEMENTARY MATERIALS

Supplementary material for this article is available at http://advances.sciencemag.org/cgi/content/full/5/11/eaav3097/DC1

Fig. S1. Transfer curves of OTFTs.
Fig. S2. Strain and stress curves of a blend film.
Fig. S3. Poisson's ratio of blend film.
Fig. S4. Rheology analysis of the blend film as a function of frequency.
Fig. S5. Rheology study of blend film as a function of temperature.
Fig. S6. Differential scanning calorimetry curves of the blended film.
Fig. S7. Stress-relaxation result of the blend film.
Fig. S8. Recovery test of an elongated blend film.
Fig. S9. TEM images of blend film as a function of blend ratio (semiconductor:elastomer).
Fig. S10. Polarized UV-vis spectra.
Fig. S11. Grazing-incidence wide-angle x-ray scattering patterns.
Fig. S12. Grazing-incidence wide-angle x-ray scattering patterns.
Fig. S13. Output and transfer curves of OTFT.
Fig. S14. Stretching test of blend film.
Fig. S15. Durability test of blend film on strain.
Fig. S16. Strain and stress curve of bulk blend film after self-healing.
Fig. S17. Transfer curves of all pixels in the 5 × 5 fully stretchable active-matrix OTFT array.
Fig. S18. Transfer curves of active-matrix sensory transistor and normalized on-current.
Fig. S19. Simulation results of maximum principal strain (e_1), intermediate principal strain (e_2), and minimum principal strain (e_3) applied by poking the stretchable active-matrix array.
Fig. S20. Fabrication process of PDMS dielectric layer for a stretchable transistor.
Table S1. On-currents of active-matrix transistor array for measurement of normalized on-current mapping of the poked transistor array.

REFERENCES AND NOTES

1. B. Yu, S.-Y. Kang, A. Akthakul, N. Ramadurai, M. Pilkenton, A. Patel, A. Nashat, D. G. Anderson, F. H. Sakamoto, B. A. Gilchrest, R. R. Anderson, R. Langer, An elastic second skin. *Nat. Mater.* **15**, 911–918 (2016).
2. S. Baik, D. W. Kim, Y. Park, T. J. Lee, S. Ho Bhang, C. Pang, A wet -tolerant adhesive patch inspired by protuberances in suction cups of octopi. *Nature* **546**, 396–400 (2017).
3. B. C.-K. Tee, A. Chortos, A. Berndt, A. K. Nguyen, A. Tom, A. McGuire, Z. C. Lin, K. Tien, W.-G. Bae, H. Wang, P. Mei, H.-H. Chou, B. Cui, K. Deisseroth, T. N. Ng, Z. Bao, A skin-inspired organic digital mechanoreceptor. *Science* **350**, 313–316 (2015).
4. D. H. Kim, N. S. Lu, R. Ma, Y. S. Kim, R. H. Kim, S. D. Wang, J. Wu, S. M. Won, H. Tao, A. Islam, K. J. Yu, T. I. Kim, R. Chowdhury, M. Ying, L. Z. Xu, M. Li, H. J. Chung, H. Keum, M. McCormick, P. Liu, Y.-W. Zhang, F. G. Omenetto, Y. G. Huang, T. Coleman, J. A. Rogers, Epidermal electronics. *Science* **333**, 838–843 (2011).
5. A. Chortos, J. Liu, Z. Bao, Pursuing prosthetic electronic skin. *Nat. Mater.* **15**, 937–950 (2016).
6. J. Y. Oh, S. Rondeau-Gagné, Y.-C. Chiu, A. Chortos, F. Lissel, G.-J. N. Wang, B. C. Schroeder, T. Kurosawa, J. Lopez, T. Katsumata, J. Xu, C. Zhu, X. Gu, W.-G. Bae, Y. Kim, L. Jin, J. W. Chung, J. B.-H. Tok, Z. N. Bao, Intrinsically stretchable and healable semiconducting polymer for organic transistors. *Nature* **539**, 411–415 (2016).
7. D. Son, J. Lee, S. Qiao, R. Ghaffari, J. Kim, J. E. Lee, C. Song, S. J. Kim, D. J. Lee, S. W. Jun, S. Yang, M. Park, J. Shin, K. Do, M. Lee, K. Kang, C. S. Hwang, N. Lu, T. Hyeon, D.-H. Kim, Multifunctional wearable devices for diagnosis and therapy of movement disorders. *Nat. Nanotechnol.* **9**, 397–404 (2014).
8. B. Zhu, H. Wang, Y. Liu, D. Qi, Z. Liu, H. Wang, J. Yu, M. Sherburne, Z. Wang, X. Chen, Skin-inspired Haptic Memory Arrays with Electrically Reconfigurable Architecture. *Adv. Mater.* **28**, 1559–1566 (2016).
9. M. Kaltenbrunner, T. Sekitani, J. Reeder, T. Yokota, K. Kuribara, T. Tokuhara, M. Drack, R. Schwodiauer, I. Graz, S. Bauer-Gogonea, S. Bauer, T. Someya, An ultra-lightweight design for imperceptible plastic electronics. *Nature* **499**, 458–463 (2013).
10. K. Takei, T. Takahashi, J. C. Ho, H. Ko, A. G. Gillies, P. W. Leu, R. S. Fearing, A. Javey, Nanowire active-matrix circuitry for low-voltage macroscale artificial skin. *Nat. Mater.* **9**, 821–826 (2010).
11. D. Wirthl, R. Pichler, M. Drack, G. Kettlguber, R. Moser, R. Gerstmayr, F. Hartmann, E. Bradt, R. Kaltseis, C. M. Siket, S. E. Schausberger, S. Hild, S. Bauer, M. Kaltenbrunner, Instant tough bonding of hydrogels for soft machines and electronics. *Sci. Adv.* **3**, e1700053 (2017).
12. D. J. Lipomi, M. Vosgueritchian, B. C. K. Tee, S. L. Hellstrom, J. A. Lee, C. H. Fox, Z. Bao, Skin-like pressure and strain sensors based on transparent elastic films of carbon nanotubes. *Nat. Nanotechnol* **6**, 788–792 (2011).
13. H. Zhao, K. O'brien, S. Li, R. F. Shepherd, Optoelectronically innervated soft prosthetic hand via stretchable optical waveguides. *Sci. Robot.* **1**, eaai7529 (2016).
14. D. Rus, M. T. Tolley, Design, fabrication and control of soft robots. *Nature* **521**, 467–475 (2015).
15. J. A. Rogers, M. G. Lagally, R. G. Nuzzo, Synthesis, assembly and applications of semiconductor nanomembranes. *Nature* **477**, 45–53 (2011).
16. K.-I. Jang, K. Li, H. U. Chung, S. Xu, H. N. Jung, Y. Yang, J. W. Kwak, H. H. Jung, J. Song, C. Yang, A. Wang, Z. Liu, J. Y. Lee, B. H. Kim, J.-H. Kim, J. Lee, Y. Yu, B. J. Kim, H. Jang, K. J. Yu, J. Kim, J. W. Lee, J.-W. Jeong, Y. M. Song, Y. Huang, Y. Zhang, J. A. Rogers, Self-assembled three dimensional network designs for soft electronics. *Nat. Commun.* **8**, 15894 (2017).
17. M. Ha, S. Lim, J. Park, D.-S. Um, Y. Lee, H. Ko, Bioinspired interlocked and hierarchical design of zno nanowire arrays for static and dynamic pressure-sensitive electronic skins. *Adv. Funct. Mater.* **25**, 2841–2849 (2015).
18. G. Y. Bae, S. W. Pak, D. Kim, G. Lee, D. H. Kim, Y. Chung, K. Cho, Linearly and highly pressure-sensitive electronic skin based on a bioinspired hierarchical structural array. *Adv. Mater.* **28**, 5300–5306 (2016).
19. W. Xu, S.-Y. Min, H. Hwang, T.-W. Lee, Organic core-sheath nanowire artificial synapses with femtojoule energy consumption. *Sci. Adv.* **2**, e1501326 (2016).
20. T. Takahashi, Z. Yu, K. Chen, D. Kiriya, C. Wang, K. Takei, H. Shiraki, T. Chen, B. Ma, A. Javey, Carbon nanotube active-matrix backplanes for mechanically flexible visible light and X-ray imagers. *Nano Lett.* **13**, 5425–5430 (2013).
21. S. Lee, A. Reuveny, J. Reeder, S. Lee, H. Jin, Q. Liu, T. Yokota, T. Sekitani, T. Isoyama, Y. Abe, Z. Suo, T. Someya, A transparent bending-insensitive pressure sensor. *Nat. Nanotechnol.* **11**, 472–478 (2016).
22. S. Wang, J. Xu, W. Wang, G.-J. N. Wang, R. Rastak, F. Molina-Lopez, J. W. Chung, S. Niu, V. R. Feig, J. Lopez, T. Lei, S.-K. Kwon, Y. Kim, A. M. Foudeh, A. Ehrlich, A. Gasperini, Y. Yun, B. Murmann, J. B.-H. Tok, Z. Bao, Skin electronics from scalable fabrication of an intrinsically stretchable transistor array. *Nature* **555**, 83–88 (2018).
23. C. Wang, D. Hwang, Z. Yu, K. Takei, J. Park, T. Chen, B. Ma, A. Javey, User-interactive electronic skin for instantaneous pressure visualization. *Nat. Mater.* **12**, 899–904 (2013).
24. T. Sekitani, T. Yokota, U. Zschieschang, H. Klauk, S. Bauer, K. Takeuchi, M. Takamiya, T. Sakurai, T. Someya, Organic nonvolatile memory transistors for flexible sensor arrays. *Science* **326**, 1516–1519 (2009).
25. J. Kim, D. Son, M. Lee, C. Song, J.-K. Song, J. H. Koo, D. J. Lee, H. J. Shim, J. H. Kim, M. Lee, T. Hyeon, D.-H. Kim, A wearable multiplexed silicon nonvolatile memory array using nanocrystal charge confinement. *Sci. Adv.* **2**, e1501101 (2016).
26. J. Viventi, D.-H. Kim, L. Vigeland, E. S. Frechette, J. A. Blanco, Y.-S. Kim, A. E. Avrin, V. R. Tiruvadi, S.-W. Hwang, A. C. Vanleer, D. F. Wulsin, K. Davis, C. E. Gelber, L. Palmer, J. Van der Spiegel, J. Wu, J. Xiao, Y. Huang, D. Contreras, J. A. Rogers, B. Litt, Flexible, foldable, actively multiplexed, high-density electrode array for mapping brain activity in vivo. *Nat. Neurosci.* **14**, 1599–1605 (2011).
27. Y. Yang, M. W. Urban, Self-healing polymeric materials. *Chem. Soc. Rev.* **42**, 7446–7467 (2013).
28. N. Holten-Andersen, M. J. Harrington, H. Birkedal, B. P. Lee, P. B. Messersmith, K. Y. C. Lee, J. H. Waite, pH-induced metal-ligand cross-links inspired by mussel yield self-healing polymer networks with near-covalent elastic moduli. *Proc. Natl. Acad. Sci.* **108**, 2651–2655 (2011).
29. L. Yuan, S. Huang, Y. Hu, Y. Zhang, A. Gu, G. Liang, G. Chen, Y. Gao, S. Nutt, Poly(phenylene oxide) modified cyanate resin for self-healing. *Polym. Adv. Technol.* **25**, 752–759 (2014).
30. C.-H. Li, C. Wang, C. Keplinger, J. L. Zuo, L. Jin, Y. Sun, P. Zheng, Y. Cao, F. Lissel, C. Linder, X.-Z. You, Z. Bao, A highly stretchable autonomous self-healing elastomer. *Nat. Chem.* **8**, 618–624 (2016).
31. Y. Huang, M. Zhong, Y. Huang, M. Zhu, Z. Pei, Z. Wang, Q. Xue, X. Xie, C. Zhi, A self-healable and highly stretchable supercapacitor based on a dual crosslinked polyelectrolyte. *Nat. Commun.* **6**, 10310 (2015).

32. C. Gong, J. Liang, W. Hu, X. Niu, S. Ma, T. H. Hahn, Q. Pei, A healable, semitransparent silver nanowire-polymer composite conductor. *Adv. Mater.* **25**, 4186–4191 (2013).
33. J. P. Li, J. J. Liang, L. Li, F. B. Ren, W. Hu, J. Li, S. H. Qi, Q. B. Pei, Healable capacitive touch screen sensors based on transparent composite electrodes comprising silver nanowires and a Furan/Maleimide Diels-Alder cycloaddition polymer. *ACS Nano* **8**, 12874–12882 (2014).
34. H. Wang, B. Zhu, W. Jiang, Y. Yang, W. R. Leow, X. Chen, A mechanically and electrically self-healing supercapacitor. *Adv. Mater.* **26**, 3638–3643 (2014).
35. A. J. Bandodkar, C. S. López, A. M. V. Mohan, L. Yin, R. Kumar, J. Wang, All-printed magnetically self-healing electrochemical devices. *Sci. Adv.* **2**, e1601465 (2016).
36. T.-P. Huynh, H. Haick, Self-healing, fully functional, and multiparametric flexible sensing platform. *Adv. Mater.* **28**, 138–143 (2016).
37. P. Cordier, F. Tournilhac, C. Soulié-Ziakovic, L. Leibler, Self-healing and thermoreversible rubber from supramolecular assembly. *Nature* **451**, 977–980 (2008).
38. E. Palleau, S. Reece, S. C. Desai, M. E. Smith, M. D. Dickey, Self-healing stretchable wires for reconfigurable circuit wiring and 3D microfluidics. *Adv. Mater.* **25**, 1589–1592 (2013).
39. J. Herrmann, K.-H. Müller, T. Reda, G. R. Baxter, B. Raguse, G. J. J. B. de Groot, R. Chai, M. Roberts, L. Wieczorek, Nanoparticle films as sensitive strain gauges. *Appl. Phys. Lett.* **91**, 183105 (2007).
40. M. Park, J. Im, M. Shin, Y. Min, J. Park, H. Cho, S. Park, M. B. Shim, S. Jeon, D.-Y. Chung, J. Bae, J. Park, U. Jeong, K. Kim, Highly stretchable electric circuits from a composite material of silver nanoparticles and elastomeric fibres. *Nat. Nanotechnol.* **7**, 803–809 (2012).
41. H. Nesser, J. Grisolia, T. Alnasser, B. Viallet, L. Ressier, Towards wireless highly sensitive capacitive strain sensors based on gold colloidal nanoparticles. *Nanoscale* **10**, 10479–10487 (2018).
42. S. Choi, S. I. Han, D. Jung, H. J. Hwang, C. Lim, S. Bae, O. K. Park, C. M. Tschabrunn, M. Lee, S. Y. Bae, J. W. Yu, J. H. Ryu, S.-W. Lee, K. Park, P. M. Kang, W. B. Lee, R. Nezafat, T. Hyeon, D.-H. Kim, Highly conductive, stretchable and biocompatible Ag–Au core–sheath nanowire composite for wearable and implantable bioelectronics. *Nat. Nanotechnol.* **13**, 1048–1056 (2018).
43. X. Yan, Z. Liu, Q. Zhang, J. Lopez, H. Wang, H.-C. Wu, S. Niu, H. Yan, S. Wang, T. Lei, J. Li, D. Qi, P. Huang, J. Huang, Y. Zhang, Y. Wang, G. Li, J. B.-H. Tok, X. Chen, Z. Bao, Quadruple H-bonding cross-linked supramolecular polymeric materials as substrates for stretchable, antitearing, and self-healable thin film electrodes. *J. Am. Chem. Soc.* **140**, 5280–5289 (2018).
44. Y. Kim, J. Zhu, B. Yeom, M. Di Prima, X. Su, J.-G. Kim, S. J. Yoo, C. Uher, N. A. Kotov, Stretchable nanoparticle conductors with self-organized conductive pathways. *Nature* **500**, 59–63 (2013).
45. S. E. Root, S. Savagatrup, A. D. Printz, D. Rodriquez, D. J. Lipomi, Mechanical properties of organic semiconductors for stretchable, highly flexible, and mechanically robust electronics. *Chem. Rev.* **117**, 6467–6499 (2017).
46. P. M., Parker, *Polydimethylsiloxane: Webster's Timeline History, 1968–2007* (ICON Group International, 2009).
47. C. S. Boland, U. Khan, G. Ryan, S. Barwich, R. Charifou, A. Harvey, C. Backes, Z. Li, M. S. Ferreira, M. E. Möbius, R. J. Young, J. N. Coleman, Sensitive electromechanical sensors using viscoelastic graphene-polymer nanocomposites. *Science* **354**, 1257–1260 (2016).
48. Z. Liu, D. Qi, P. Guo, Y. Liu, B. Zhu, H. Yang, Y. Liu, B. Li, C. Zhang, J. Yu, B. Liedberg, X. Chen, Thickness-gradient films for high gauge factor stretchable strain sensors. *Adv. Mater.* **27**, 6230–6237 (2015).
49. D. Kang, P. V. Pikhitsa, Y. W. Choi, C. Lee, S. S. Shin, L. Piao, B. Park, K. Y. Suh, T. I. Kim, M. Choi, Ultrasensitive mechanical crack-based sensor inspired by the spider sensory system. *Nature* **516**, 222–226 (2014).
50. X. Li, R. Zhang, W. Yu, K. Wang, J. Wei, D. Wu, A. Cao, Z. Li, Y. Cheng, Q. Zheng, R. S. Ruoff, H. Zhu, Stretchable and highly sensitive graphene-on-polymer strain sensors. *Sci. Rep.* **2**, 870 (2012).
51. Z. Liu, X. Wang, D. Qi, C. Xu, J. Yu, Y. Liu, Y. Jiang, B. Liedberg, X. Chen, High-adhesion stretchable electrodes based on nanopile interlocking. *Adv. Mater.* **29**, 1603382 (2017).
52. S. P. Lacour, D. Chan, S. Wagner, T. Li, Z. Suo, Mechanisms of reversible stretchability of thin metal films on elastomeric substrates. *Appl. Phys. Lett.* **88**, 204103 (2006).
53. Y. Ito, A. A. Virkar, S. Mannsfeld, J. H. Oh, M. Toney, J. Locklin, Z. A. Bao, Crystalline ultrasmooth self-assembled monolayers of alkylsilanes for organic field-effect transistors. *J. Am. Chem. Soc.* **131**, 9396–9404 (2009).
54. J. L. Baker, L. H. Jimison, S. Mannsfeld, S. Volkman, S. Yin, V. Subramanian, A. Salleo, A. P. Alivisatos, M. F. Toney, Quantification of thin film crystallographic orientation using X-ray diffraction with an area detector. *Langmuir* **26**, 9146–9151 (2010).
55. R. W. Ogden, Large deformation isotropic elasticity – on the correlation of theory and experiment for incompressible rubberlike solids. *Proc. R. Soc. A.* **326**, 565–584 (1972).
56. R. W. Ogden, Large deformation isotropic elasticity – on the correlation of theory and experiment for the compressible rubberlike solids. *Proc. R. Soc. A.* **328**, 567–583 (1972).

Acknowledgments: J.Y.O. acknowledges the partial support from the National Research Foundation of Korea (NRF) grant funded by the Korea government (NRF-2019R1A1062160). **Funding:** J.Y.O. and D.S were supported by Samsung Electronics. J.L. acknowledges support by the National Science Foundation Graduate Research Fellowship Program under grant no. DGE-114747. N.G.-J.W. was supported by Department of Defense Air Force Office of Scientific Research (grant no. FA9550-18-1-0143). Part of this work was performed at the Stanford Nano Shared Facilities (SNSF), supported by the National Science Foundation under award ECCS-1542152. **Author contributions:** J.Y.O., D.S., T.K., and Z.B. conceived and designed the experiments. J.Y.O., D.S., T.K., Y.L., Y.K. J.L., H.-C.W., J.K., J.P., X.G., J.M., N.G.-J.W., Y. Yin, W.C., Y. Yun, J.B.-H.T., and Z.B. performed experiments and analysis. J.Y.O., D.S., T.K., J.B.-H.T., and Z.B. wrote the manuscript. **Competing interests:** J.Y.O., D.S., T.K., Y.Y, and Z.B. are inventors on a provisional U.S. patent application related to this work (serial no. 62/677,239, filed on 28 May 2018). The other authors declare that they have no competing interests. **Data and materials availability:** All data needed to evaluate the conclusions in the paper are present in the paper and/or the Supplementary Materials. Additional data related to this paper may be requested from the authors.

Submitted 4 September 2018
Accepted 16 September 2019
Published 8 November 2019
10.1126/sciadv.aav3097

Citation: J. Y. Oh, D. Son, T. Katsumata, Y. Lee, Y. Kim, J. Lopez, H.-C. Wu, J. Kang, J. Park, X. Gu, J. Mun, N. G.-J. Wang, Y. Yin, W. Cai, Y. Yun, J. B.-H. Tok, Z. Bao, Stretchable self-healable semiconducting polymer film for active-matrix strain-sensing array. *Sci. Adv.* **5**, eaav3097 (2019).